




Communication

Photoreduction of Copper Ions Using Silica–Surfactant Hybrid and Titanium (IV) Oxide under Sulfuric Acid Conditions

Shingo Machida ^{1,*}, Reo Kato ¹, Kaishi Hasegawa ¹, Takahiro Gotoh ², Ken-ichi Katsumata ¹
and Atsuo Yasumori ¹

¹ Department of Material Science and Technology, Faculty of Advanced Engineering, Tokyo University of Science, 6-3-1 Niijuku, Katsushika-ku, Tokyo 125-8585, Japan; 8218b03@alumni.tus.ac.jp (R.K.); 8221543@ed.tus.ac.jp (K.H.); k.katsumata@rs.tus.ac.jp (K.-i.K.); yasumori@rs.tus.ac.jp (A.Y.)

² Material Characterization Central Laboratory, School of Science and Engineering, Waseda University, 3-4-1 Okubo, Shinjuku-ku, Tokyo 169-8555, Japan; tgotoh@waseda.jp

* Correspondence: shingo.machida@rs.tus.ac.jp

Abstract: Photoreduction of Cu²⁺ ions to Cu metal by titanium(IV) oxide (TiO₂) was conducted in the presence of a silica–surfactant hybrid under sulfuric acid conditions. After irradiation, a dark-red color, reflections due to Cu metal in the X-ray diffraction pattern, and peaks due to Cu 2p_{1/2} and 2p_{3/2} in the X-ray photoelectron spectrum indicated the precipitation of Cu metal in the product. In addition, an increase in the Brunauer–Emmett–Teller specific surface area from 36 and 45 m²/g for the silica–surfactant and TiO₂, respectively, to 591 m²/g for the product, and a decrease in the intensity of the C–H stretching band in the Fourier–transform infra-red spectra implied the removal of surfactant during the reaction. These characteristics were never observed when TiO₂ was used solely. Therefore, this study indicated that the photoreduction of Cu²⁺ ions to Cu metal by TiO₂ was facilitated under the sulfuric acid medium, where the surfactants extracted from silica–surfactant hybrids by protons in the acidic condition were successfully photo-oxidized by TiO₂. Thus, this study presents a new application of the conversion of a silica–surfactant hybrid into mesoporous silicas.

Keywords: mesoporous silica; silica–surfactant hybrid; heavy metal ion; photoreduction; titanium oxide



Citation: Machida, S.; Kato, R.; Hasegawa, K.; Gotoh, T.; Katsumata, K.-i.; Yasumori, A. Photoreduction of Copper Ions Using Silica–Surfactant Hybrid and Titanium (IV) Oxide under Sulfuric Acid Conditions. *Materials* **2022**, *15*, 5132. <https://doi.org/10.3390/ma15155132>

Academic Editor: Francesco Baino

Received: 6 June 2022

Accepted: 19 July 2022

Published: 24 July 2022

Publisher's Note: MDPI stays neutral with regard to jurisdictional claims in published maps and institutional affiliations.



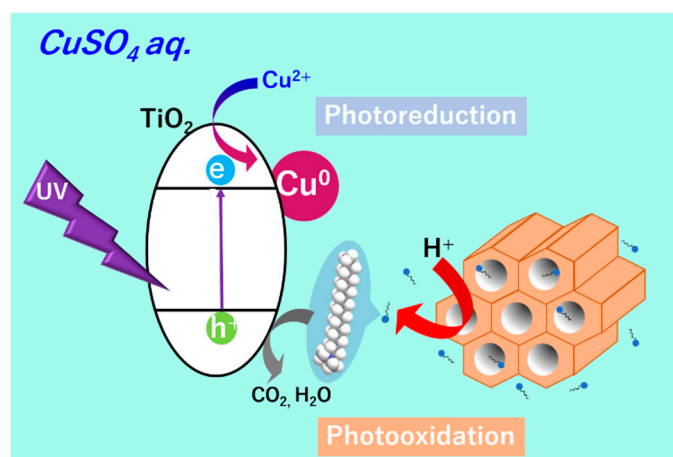
Copyright: © 2022 by the authors. Licensee MDPI, Basel, Switzerland. This article is an open access article distributed under the terms and conditions of the Creative Commons Attribution (CC BY) license (<https://creativecommons.org/licenses/by/4.0/>).

1. Introduction

The discovery of mesoporous silicas prepared by a supramolecular templating approach in the 1990s [1,2] prompted studies of their fundamental properties and practical applications, leading to the generation of mesoporous silicas with varied mesostructures that originated from the mesostructures of silica–surfactant hybrids that form via self-assembly of surfactants such as alkyltrimethylammonium salts with concurrent silica precipitation [1–7]. Thus, porous structures form upon removal of the surfactants via calcination using an electric furnace or via acid extraction under mild conditions [1–7]. The former process can emit carbon dioxide gas, whereas the latter process proceeds under mild conditions but generates a waste solvent that contains surfactants. Therefore, we focused on adding this surfactant-containing waste to wastewater to promote the removal of pollutants for environmental purification applications. Notably, mesoporous silicas that release surfactants can be used as adsorbents to purify waste water [6,7].

Here, we report the photoreduction of Cu²⁺ ions using silica–surfactant hybrids and titanium (IV) oxide (TiO₂) under sulfuric acid conditions (Scheme 1). Specifically, photoreduction of heavy-metal ions was conducted with the concurrent oxidation of surfactants by combining TiO₂ with silica–surfactant hybrids. TiO₂ is an extensively studied photocatalyst [8–10] that promotes the photo-oxidation of organic compounds and the photoreduction of heavy-metal ions to metals [8–11]. The latter process can be used to produce visible-light-responsive photocatalysts and antibacterial materials [8–11], and the generated heavy metals can be photo-oxidized by TiO₂ [12]. Notably, heavy-metal ions

are present in sulfuric-acid-containing wastewater from mines [13,14]. Sulfate ions can be adsorbed onto the surface of TiO_2 to decrease its photocatalytic activity [15]. Therefore, surfactants extracted from silica–surfactant hybrids by sulfuric acid are promising organic compounds that can be degraded by photo-oxidation by TiO_2 , promoting the photoreduction of heavy-metal ions by TiO_2 in the presence of sulfuric acid. Thus, the photocatalytic activity of TiO_2 has the potential to both degrade surfactants present as additional waste and remove heavy-metal ions as metal precipitates.



Scheme 1. An overview of the present study.

2. Material and Methods

Copper(II) sulfate (CuSO_4) pentahydrate and methanol were obtained from Wako Pure Chemical. Tetraethoxysilane (TEOS) and hexadecyltrimethylammonium chloride (C16TAC) were obtained from TCI. A 28 wt% ammonia solution was obtained from Kanto Chemical (Tokyo, Japan). All the chemicals were reagent grade and used without further purification.

In the present study, we conducted photoreduction of Cu^{2+} ions because their concentration is easily measured and estimated by UV–vis spectrophotometric analysis of the well-known blue-colored complex $[\text{Cu}(\text{NH}_3)_4]^{2+}$ [16]. To easily determine the particle morphology, in accordance with a previous study [17], we prepared spherical silica–surfactant hybrid particles via homogeneous precipitation of both silica and C16TAC in a methanolic solution containing ammonia. After TEOS was added to the methanol/water mixture containing ammonia (the TEOS:C16TAC:H₂O:methanol:ammonia molar ratio was 1:0.4:774:1501:72 in the initial dispersion), the solution was shaken for 3 s and aged at room temperature for 20 h. After the reaction, the resultant solid was centrifuged, washed with methanol, and then dried for 80 °C for 1 day. A field-emission scanning electron microscopy (FE-SEM) image of the product is shown in Figure 1. For comparison, the as-synthesized spherical particles (ASP) were calcined at 550 °C for 20 h, similar to the procedure used in a previous study [17] to prepare calcined spherical particles (CSP) as a nanoporous silica. The TiO_2 was a standard photocatalyst (P25, Degussa, Düsseldorf, Germany). After both P25 (20 mg) and ASP (80 mg) were dispersed in a 10 mmol/L CuSO_4 solution (5 mL) adjusted to pH 4 by the addition of sulfuric acid, the dispersion was irradiated with a He–Xe lamp for 4 h through a quartz plate. The irradiation area was the same as the width of the reaction vessel, and the distance between the top of the dispersion (whose height from the bottom of the reaction vessel was 1 cm) and the lamp was 0.5 cm. During irradiation, the dispersion was briefly stirred for every hour. The dispersion was also continuously stirred for comparison purposes. After the reaction, the resultant solid was centrifuged at 5000 rpm for 10 min and then washed with distilled water, to obtain the product denoted herein as Cu–P25–ASP. The resultant supernatant showed an increase in pH from 4 to 5 and contained bubbles on its surface, a common feature of surfactant aqueous solutions. The obtained solid was dried under a reduced pressure for 1 day. For comparison, these

procedures were also applied to separate starting solutions containing P25 (20 mg), ASP (80 mg), and C16TAC (20 mg) individually.

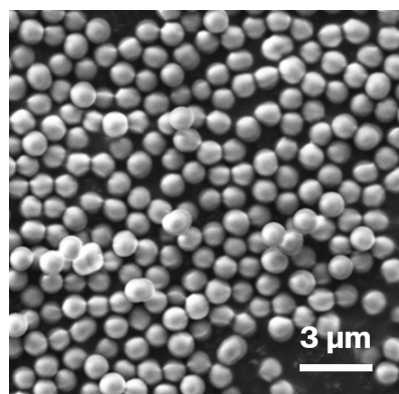


Figure 1. FE-SEM image of ASP.

3. Results and Discussion

After irradiation, the P25–ASP mixed dispersion was dark-red (Figure 2), whereas the dispersions of P25 or ASP and the solution of C16TAC containing Cu^{2+} were not. Notably, when the P25–ASP mixed dispersion was continuously stirred, the red coloration was not observed. Because the powders used in the present study did not immediately settle in the reaction vessel, UV light likely did not reach the vessel bottom and a certain UV irradiation time was necessary to change the dispersion color. The X-ray diffraction (XRD) pattern for the Cu–P25–ASP shows reflections attributable to P25 and ASP as well as Cu metal; no reflections attributable to copper oxides are observed (Figure 3). Transmission electron microscopy (TEM) and scanning TEM (STEM) images of the Cu–P25–ASP show spherical particles (ASP) and ~ 30 nm particles of P25. The latter particles exhibit relatively dark and bright regions (Figure 4a,b). The light regions contain high concentrations of Cu, as evident in the corresponding energy-dispersive X-ray (EDX) mapping image (Figure 4d). In addition, the spherical particles and the ~ 30 nm particles of P25 contain Si and Ti, as revealed in the EDX mapping images, respectively (Figure 4e,f). The X-ray photoelectron spectrum of the Cu–P25–ASP (Figure 5) shows peaks at binding energies of 953.5, 943.0, 933.0, and 932.5 eV, which are attributed to Cu $2p_{1/2}$, Cu $^{2+}$ satellite, Cu $^{2+}$ $2p_{3/2}$, and Cu $2p_{3/2}$, respectively [18,19]. The ratios of the decrease in Cu $^{2+}$ concentration relative to those in the starting solutions are reported in Table 1. The dispersion that contained both P25 and ASP resulted in the largest decrease, whereas the Cu $^{2+}$ concentration hardly decreased for the P25 dispersion or the C16TAC solution. In contrast, the ASP dispersion resulted in a 40% decrease in Cu $^{2+}$ concentration.

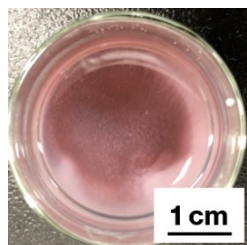


Figure 2. Photograph of Cu–P25–ASP.

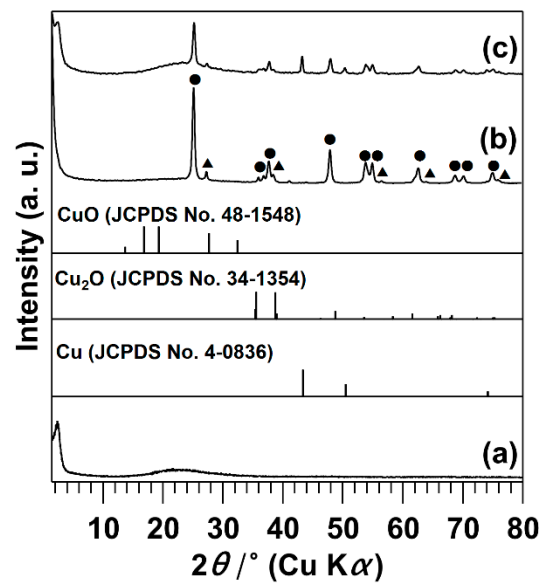


Figure 3. XRD patterns for (a) ASP, (b) P25, and (c) Cu-P25-ASP. Filled triangles and circles denote anatase and rutile reflections, respectively.

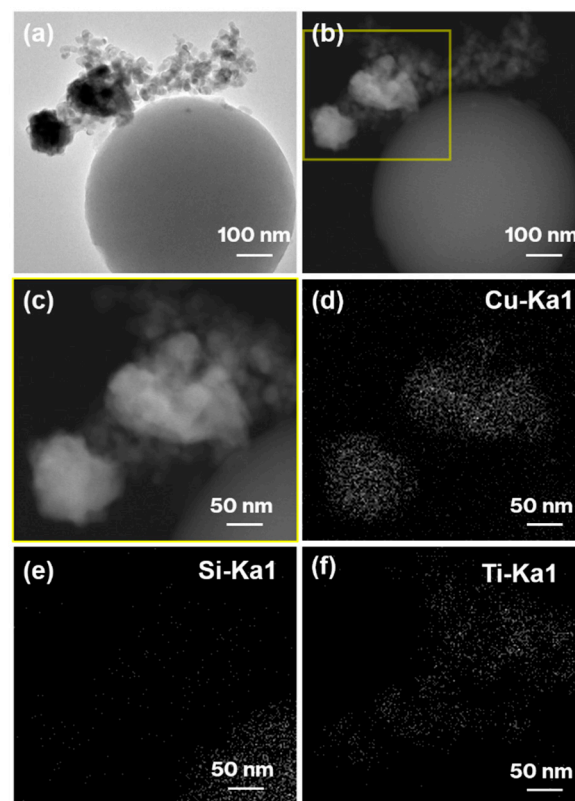


Figure 4. (a) TEM and (b) STEM images of Cu-P25-ASP. The region indicated by the yellow square in (b) is enlarged in (c). EDX mapping image for Cu, Si, and Ti in figure (c) are shown in figures (d–f), respectively.

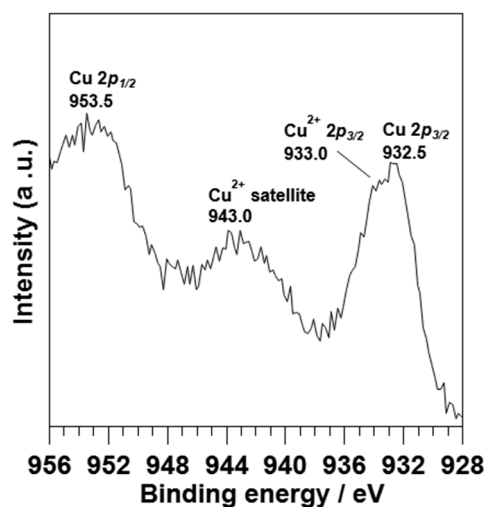


Figure 5. XPS spectrum of Cu-P25-ASP.

Table 1. Ratios reflecting the decrease in Cu^{2+} concentration after irradiation of the additives combined with the starting solution.

Additives	Cu^{2+} Decrease Ratios (%)
P25 + ASP	48
P25	0.010
ASP	40
C16TAC	2.5

The intensities of the C–H stretching bands [20] at 2922 and 2872 cm^{-1} and the C–N stretching band [20] at 1460 cm^{-1} in the Fourier transform infrared (IR) spectrum of the solid mixture of P25 (20 mg) and ASP (80 mg) are substantially lower than those in the spectrum of the Cu-P25-ASP (Figure 6). Based on the CHN analyses, the C and N contents (2.9 and 0.13 mass%, respectively) in the Cu-P25-ASP are lower than those in the mixed solid before irradiation (18 and 0.95 mass%, respectively). Figure 7 shows N_2 adsorption/desorption isotherms for the ASP, P25, Cu-P25-ASP, and CSP, recorded at -196 °C. Based on these isotherms, the specific surface areas of the ASP, P25, Cu-P25-ASP, and CSP were calculated to be 36, 45, 591, and 806 m^2/g using the Brunauer–Emmett–Teller (BET) method [21]. These BET surface areas, the Barrett–Joyner–Halenda (BJH) [22] pore sizes, and the pore volumes estimated using the BJH method are listed in Table 2 for Cu-P25-ASP and CSP.

Table 2. List of BET surface areas, BJH pore sizes, or pore volumes for ASP, P25, Cu-P25-ASP, and CSP.

Samples	BET Surface Area (m^2/g)	BJH Pore Size (nm)	Pore Volume (cm^3/g)
ASP	36	-	-
P25	45	-	-
Cu-P25-ASP	591	1.2	0.11
CSP	806	1.2	0.18

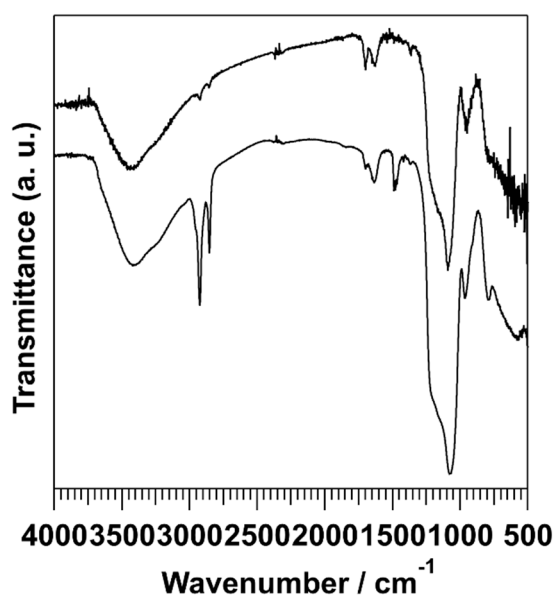


Figure 6. IR spectra of ASP-P25 mixed solid (bottom) and Cu-P25-ASP (top).

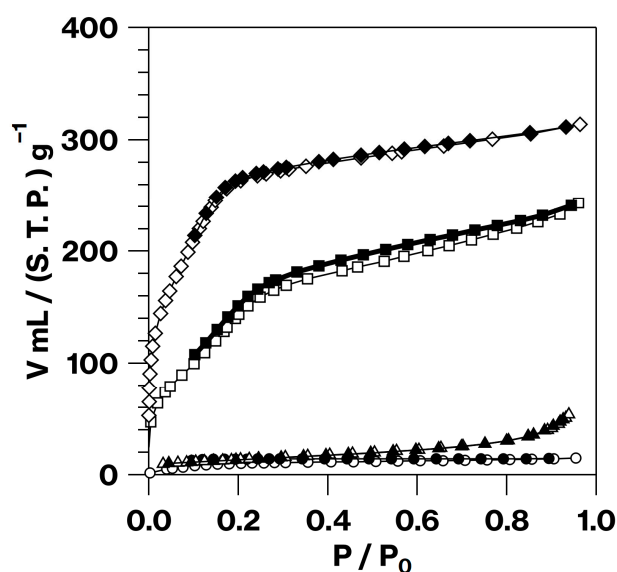


Figure 7. N₂ adsorption/desorption isotherms for ASP (circles), P25 (triangles), C25P25-ASP (squares), and CSP (diamonds). Open and filled symbols represent adsorption and desorption, respectively. The solid lines are visual aids.

Collectively, the product appearance (Figure 2), XRD patterns (Figure 3), XPS spectrum (Figure 5), and electron microscopy and elemental analysis results (Figure 4) reveal that Cu²⁺ was photo-reduced, resulting in the precipitation of Cu metal in the P25-ASP mixed product after irradiation. Copper oxides are absent, consistent with the lower redox potential of the conduction band of TiO₂ (−0.52 V) [8] relative to those for Cu²⁺/Cu⁺ (0.15 V), Cu²⁺/Cu (0.34 V), and for Cu⁺/Cu (0.52 V) [23].

Alkylammonium ions are well known to be degraded by •OH and •O₂ radicals, which can be generated by reaction of H₂O and O₂ molecules with holes photogenerated in the valence band of TiO₂ [24]. In the present study, the IR spectra, N₂ adsorption/desorption isotherms (Figure 7), and elemental analyses indicate a decrease in the concentration of hexadecyltrimethylammonium ions (C16TMA⁺) in the ASP after the reaction. Because a decrease in the concentration of Cu²⁺ was observed when ASP alone was used for the present reaction (Table 1) and because the cation-exchange reactions of silanol groups on

silicas are well known [25], exchange reactions of C16TMA⁺ with protons and/or Cu²⁺ ions in the CuSO₄ acidic solution are highly likely, as indicated by an increase in the pH of the dispersion after the reaction (see Material and Methods). The presence of Cu²⁺ detected by XPS (Figure 5) thus results from Cu²⁺ ions adsorbed onto the ASP, which are not accessible on P25 surfaces (Figure 4) or on the white regions observed after irradiation (Figure 2); the latter situation can be improved by modifying the experimental conditions. The dispersion never became dark-red as shown in Figure 2 when the present reaction was conducted with P25 alone; it remained white. In addition, the Cu²⁺ decrease ratio for the Cu–P25–ASP is higher than those for the P25 and ASP. Notably, the solution after irradiation was still under sulfuric acid conditions (refer to the experimental conditions). Therefore, photo-oxidation of C16TMA⁺ extracted from ASP is evident in the present reaction, and this photo-oxidation successfully promoted the photoreduction of Cu²⁺ under sulfuric acid conditions.

After the dispersion containing P25 and ASP was irradiated for 4 h, slight bubbling was observed on the surface of the dispersed particles, suggesting the presence of undegraded C16TMA⁺. In addition, C16TMA⁺ and/or C16TAC was incompletely extracted from the ASP according to the residual alkyl chains in Cu–P25–ASP, as revealed by the IR spectra and CHN analyses; this interpretation is further supported by the lower porosity of Cu–P25–ASP compared with that of CSP, as determined from the N₂ adsorption/desorption isotherms (Figure 7). Notably, silica–surfactant hybrid spheres have been prepared using alkyltrimethylammonium salts with shorter side-chain lengths [4]. In addition, the synthesis of silica–surfactant hybrids has been used to coat silica–surfactant layers onto various inorganic surfaces to form inorganic solid/silica–surfactant core–shell particles [5,17]. Increasing the amounts of TiO₂ and TiO₂-based compounds [26,27] and/or other materials [28] added to the present reaction is also feasible. Meanwhile, because the Cu²⁺ adsorption capability of P25 is low under sulfuric acid conditions (Table 1), the cation adsorption ability of TiO₂ surfaces in the presence of protons, where acid sites on TiO₂ surfaces could be strongly related to their adsorption ability, warrants further investigation [29–32]. However, the present product containing Cu metal might find applications where visible-light-responsive photocatalysts and antibacterial materials [7–14] have been used. We plan to conduct such studies in the future.

4. Conclusions

We demonstrated the photoreduction of Cu²⁺ ions to Cu metal by TiO₂ under sulfuric acid conditions, where the surfactant molecules extracted from silica–surfactant hybrid spheres were successfully photo-oxidized by TiO₂. Therefore, the present study might provide a new strategy for environmental purification, where the addition of another waste to wastewater efficiently promotes both degradation and removal of surfactants and heavy metals.

Author Contributions: S.M.: conceptualization, investigation, writing—original draft, supervision. R.K.: data curation, investigation. K.H.: data curation, investigation. T.G.: data curation, investigation. K.-i.K.: writing—review and editing, project administration. A.Y.: writing—review and editing, project administration. All authors have read and agreed to the published version of the manuscript.

Funding: This work was supported by a 36th Research Grant from Hitachi Metals-Materials Science Foundation, Japan.

Data Availability Statement: Available on request from the corresponding author.

Acknowledgments: This work was conducted using research equipment (TEM, STEM, EDX measurements) in the Materials Characterization Central Laboratory of Waseda University, which was shared in the MEXT Project for promoting public utilization of advanced research infrastructure (program for supporting the construction of core facilities, Grant No. JPMXS0440500021). Our sincere thanks to Kazuo Miyamura and Akinori Honda, and researchers at the Tokyo University of Science, who carried out the CHN measurements.

Conflicts of Interest: The authors declare no conflict of interest.

References

1. Yanagisawa, T.; Shimizu, T.; Kuroda, K.; Kato, C. The Preparation of Alkyltrimethylammonium-Kanemite Complexes and Their Conversion of Microporous Materials. *Bull. Chem. Soc. Jpn.* **1990**, *63*, 988–992. [[CrossRef](#)]
2. Kresge, C.T.; Leonowicz, M.E.; Roth, W.J.; Vartuli, J.C.; Beck, J.S. Ordered Mesoporous Molecular Sieves Synthesized by a Liquid-Crystal Template Mechanism. *Nature* **1992**, *359*, 710–712. [[CrossRef](#)]
3. Huo, Q.; Margolese, D.I.; Ciesla, U.; Demuth, D.G.; Feng, P.; Gier, T.E.; Sieger, P.; Firouzi, A.; Chmelka, B.F.; Schüth, F.; et al. Organization of Organic Molecules with Inorganic Molecular Species into Nanocomposite Biphasic Arrays. *Chem. Mater.* **1994**, *6*, 1176–1191. [[CrossRef](#)]
4. Shiba, K.; Shimura, N.; Ogawa, M. Mesoporous Silica Spherical Particles. *J. Nanosci. Nanotechnol.* **2013**, *13*, 2483–2494. [[CrossRef](#)] [[PubMed](#)]
5. Ogawa, M. Mesoporous Silica Layer: Preparation and Opportunity. *Chem. Rec.* **2017**, *17*, 217–232. [[CrossRef](#)]
6. Rastegari, E.; Hsiao, Y.-J.; Lai, W.-Y.; Lai, Y.-H.; Yang, T.-C.; Chen, S.-J.; Huang, P.-I.; Chiou, S.-H.; Mou, C.-Y.; Chien, Y. An Update on Mesoporous Silica Nanoparticles Applications in Nanomedicine. *Pharmaceutics* **2021**, *13*, 1067. [[CrossRef](#)] [[PubMed](#)]
7. AlOthman, Z.A. A Review: Fundamental Aspects of Silicate Mesoporous Materials. *Materials* **2012**, *5*, 2874–2902. [[CrossRef](#)]
8. Fujishima, A.; Rao, T.N.; Tryk, D.A. Titanium Dioxide Photocatalysis. *J. Photochem. Photobiol. C Photochem. Rev.* **2000**, *1*, 1–21. [[CrossRef](#)]
9. Nakata, K.; Fujishima, A. TiO₂ Photocatalysis: Design and Applications. *J. Photochem. Photobiol. C Photochem. Rev.* **2012**, *13*, 169–189. [[CrossRef](#)]
10. Meng, X.; Gao, X. Photocatalysis for Heavy Metal Treatment: A Review. *Processes* **2021**, *9*, 1729.
11. Liao, C.; Li, Y.; Tjong, S.C. Visible-Light Active Titanium Dioxide Nanomaterials with Bactericidal Properties. *Nanomaterials* **2020**, *10*, 124. [[CrossRef](#)] [[PubMed](#)]
12. Janczarek, M.; Kowalska, E. On the Origin of Enhanced Photocatalytic Activity of Copper-Modified Titania in the Oxidative Reaction Systems. *Catalysts* **2017**, *7*, 317. [[CrossRef](#)]
13. Tong, L.; Fan, R.; Yang, S.; Li, C. Development and Status of the Treatment Technology for Acid Mine Drainage. *Min. Metall. Explor.* **2021**, *38*, 315–327. [[CrossRef](#)]
14. Rodríguez-Galán, M.; Baena-Mreno, F.M.; Vázquez, S.; Arroyo-Torrovlo, F.; Vilches, L.F.; Zhang, Z. Remediation of Acid Mine Drainage. *Environ. Chem. Lett.* **2019**, *17*, 1529. [[CrossRef](#)]
15. Bhatkhande, D.S.; Pangarkar, V.G.; Beenackers, A.A.C.M. Photocatalytic Degradation for Environmental Applications—A Review. *J. Chem. Technol. Biotechnol.* **2002**, *77*, 102–116. [[CrossRef](#)]
16. Guspita, D.; Ulianas, A. Optimization of Complex NH₃ with Cu²⁺ Ions to Determine Levels of Ammonia by UV-Vis Spectrophotometer. *J. Phys. Conf. Ser.* **2020**, *1481*, 012040. [[CrossRef](#)]
17. Shimura, N.; Ogawa, M. Preparation of Surfactant Templated Nanoporous Silica Spherical Particles by the Stöber method. Effect of Solvent Composition on the Particle Size. *J. Mater. Sci.* **2007**, *42*, 5299–5306. [[CrossRef](#)]
18. Miyagawa, M.; Yonemura, M.; Tanaka, H. Lustrous Copper Nanoparticle Films: Photodeposition with High Quantum Yield and Electric Conductivity. *Chem. Phys. Lett.* **2016**, *665*, 95–99. [[CrossRef](#)]
19. Pallavicini, P.; Dacarro, G.; Grisoli, P.; Mangano, C.; Patrini, M.; Rigoni, F.; Sangaletti, L.; Taglietti, A. Coordination chemistry for antibacterial materials: A monolayer of a Cu₂+2,2'-bipyridine complex grafted on a glass surface. *Dalton Trans.* **2013**, *42*, 4522–4560. [[CrossRef](#)]
20. Kato, R.; Shimura, N.; Ogawa, M. Controlled Photocatalytic Ability of Titanium Dioxide Particle by Coating with Nanoporous silica. *Chem. Lett.* **2008**, *37*, 76–77. [[CrossRef](#)]
21. Brunauer, S.; Emmett, P.H.; Teller, E. Adsorption Gases in Multimolecular Layers. *J. Am. Chem. Soc.* **1938**, *407*, 309–319. [[CrossRef](#)]
22. Barret, E.P.; Joyner, L.G.; Halenda, P.P. The Determination of Pore Volume and Area Distributions in Porous Substances. I. Computations from Nitrogen Isotherms. *J. Am. Chem. Soc.* **1951**, *73*, 373–380. [[CrossRef](#)]
23. Chen, K.; Xue, D. Reaction Route to the Crystallization of Copper Oxides. *Appl. Sci. Conver. Technol.* **2014**, *23*, 14–26. [[CrossRef](#)]
24. Umemura, Y.; Shinohara, E.; Koura, A.; Nishioka, T.; Sasaki, T. Photocatalytic Decomposition of an Alkylammonium Cation in a Langmuir-Blodgett Film of a Titania Nanosheet. *Langmuir* **2006**, *22*, 3870–3877. [[CrossRef](#)]
25. Mercier, L.; Pinnavia, J. Access in Mesoporous Materials: Advanced of a Uniform Pore Structure in the Design of a Heavy Metal Ion Adsorbent for Environmental Remediation. *Adv. Mater.* **1997**, *9*, 500–503. [[CrossRef](#)]
26. Hattori, H.; Ide, Y.; Sano, T. Microporous Titanate Nanofibers for Highly Efficient UV-Protective Transparent Coating. *J. Mater. Chem. A* **2014**, *2*, 16381–16388. [[CrossRef](#)]
27. Saito, K.; Kozeni, M.; Sohmiya, M.; Komaguchi, K.; Ogawa, M.; Sugahara, Y.; Ide, Y. Unprecedentedly Enhanced Solar Photocatalytic Activity of a Layered Titanate Simply Integrated with TiO₂ Nanoparticles. *Phys. Chem. Chem. Phys.* **2016**, *18*, 30920–30925. [[CrossRef](#)]
28. Wang, Q.; Zhang, L.; Guo, Y.; Sheng, M.; Wang, M.; Li, B.; Shi, J. Multifunctional 2D porous g-C₃N₄ Nanosheets Hybridized with 3D Hierarchical TiO₂ Microflowers for Selective Dye Adsorption, Antibiotic Degradation and CO₂ Reduction. *Chem. Eng. J.* **2020**, *396*, 125347. [[CrossRef](#)]
29. Deiana, C.; Fois, E.; Coluccia, S.; Martra, G. Surface Structure of TiO₂ P25 Nanoparticles: Infrared Study of Hydroxyl Groups on Coordinative Defect Sites. *J. Phys. Chem. C* **2010**, *114*, 21531–21538. [[CrossRef](#)]

30. Lin, H.; Long, J.; Gu, Q.; Zhang, W.; Ruan, R.; Li, Z.; Wang, X. In situ IR Study of Surface Hydroxyl Species of Dehydrated TiO₂: Towards Understanding Pivotal Surface Process of TiO₂ Photocatalytic Oxidation of Toluene. *Phys. Chem. Chem. Phys.* **2012**, *14*, 9468–9474. [[CrossRef](#)]
31. Kitano, M.; Wada, E.; Nakajima, K.; Hayashi, S.; Miyazaki, S.; Kobayashi, H.; Hara, M. Protonated Titanate Nanotubes with Lewis and Brønsted Acidity: Relationship between Nanotube Structure and Catalytic Activity. *Chem. Mater.* **2013**, *25*, 385–393. [[CrossRef](#)]
32. Machida, S.; Sohmiya, M.; Ide, Y.; Sugahara, Y. Solid-State ³¹P Nuclear Magnetic Resonance Study of Interlayer Hydroxide Surfaces of Kaolinite Proved with an Interlayer Triethylphosphine Oxide Monolayer. *Langmuir* **2018**, *34*, 12694–12701. [[CrossRef](#)] [[PubMed](#)]